

Nanoscale

Accepted Manuscript



This is an *Accepted Manuscript*, which has been through the Royal Society of Chemistry peer review process and has been accepted for publication.

Accepted Manuscripts are published online shortly after acceptance, before technical editing, formatting and proof reading. Using this free service, authors can make their results available to the community, in citable form, before we publish the edited article. We will replace this *Accepted Manuscript* with the edited and formatted *Advance Article* as soon as it is available.

You can find more information about *Accepted Manuscripts* in the [Information for Authors](#).

Please note that technical editing may introduce minor changes to the text and/or graphics, which may alter content. The journal's standard [Terms & Conditions](#) and the [Ethical guidelines](#) still apply. In no event shall the Royal Society of Chemistry be held responsible for any errors or omissions in this *Accepted Manuscript* or any consequences arising from the use of any information it contains.

COMMUNICATION

In situ synthesis of NiS/Ni₃S₂ nanorod composite array on Ni foil as a FTO-free counter electrode for dye-sensitized solar cells

Cite this: DOI: 10.1039/x0xx00000x

Yongping Liao, Kai Pan*, Qingjiang Pan, Guofeng Wang, Wei Zhou, Honggang Fu*

Received 00th January 2012,
Accepted 00th January 2012

DOI: 10.1039/x0xx00000x

www.rsc.org/

NiS/Ni₃S₂ nanorod composite array that directly grows on Ni foil has been used as counter electrode for dye-sensitized solar cells, these nickel sulfide nanorods perform excellent photo-electrical conversion efficiency when comparing with conventionally noble-metal Pt electrode.

Dye-sensitized solar cells (DSSCs) are one of the most attracted photovoltaic devices due to their low-cost, easy fabrication and relative high conversion efficiency.¹⁻⁴ Typical DSSC consists of a dye-sensitized semiconductor photoanode, a redox electrolyte, and a counter electrode (CE) to collect electrons and catalyze the redox couple regeneration. The CEs are conventionally fabricated with noble metal Pt, showing excellent performance and stability. Obviously, the high cost and the scarcity of this noble metal electrode significantly restricts its large-scale manufacture.⁵ Therefore, it's imperative to develop new low-cost counter electrode materials with a relatively high conversion efficiency (η) for DSSCs.

A variety of materials such as carbon-based materials^{6,7} and conducting polymers⁸ have been used as CEs, and show good electrocatalytic activity. Recently, some transition metal oxides^{9,10}, nitrides¹¹, carbides¹² and sulfides¹³⁻¹⁷ have also been investigated as CEs due to both their preferentially electrocatalytic activity and facile fabrication processes. In this respect, nickel sulfide is one of the most efficient candidates because of having both high conductivity¹⁸ and excellent electrocatalytic activity^{19,20}. For example, NiS or Ni₃S₂ CEs have been prepared via solvothermal (hydrothermal) method and they are prospective catalysts to substitute the Pt CEs²¹⁻²³. Generally, the Ni atoms, as catalytic active sites²⁴, are relatively higher ratio in the Ni₃S₂ than that of NiS, which results in the relatively more catalytic active sites for the I₃⁻ reduction, therefore, the DSSCs based on the Ni₃S₂ shows a higher photoelectrical conversion efficiency than that of NiS. However, few works about the NiS/Ni₃S₂ composite nanojunction array for DSSCs have been reported. In this work, the NiS/Ni₃S₂ composite array have been directly grown on Ni foil and used as counter electrode for DSSCs. And high photoelectrical conversion efficiency has been obtained because NiS/Ni₃S₂ nanorod composite arrays can provide many catalytic active sites²⁴ and easier electrons transfer²⁵.

Here, a facile one-step hydrothermal method was used to prepare the NiS/Ni₃S₂ nanorod composite that directly grows on the Ni foil (see details in supporting information). Aqueous hydrazine is used to

assist the dissolution and reduction of sulfur and coordinate the nickel ions by forming the complex [Ni(N₂H₄)₃]²⁺, which led to the formation of NiS/Ni₃S₂ hybrid form. Without hydrazine, the slower dissolution of sulfur powder in water under hydrothermal treatment could not provide a sufficient amount of S²⁻. The coordination between hydrazine and nickel ions is thought to be the reason for the formation of nanorod composite arrays. In addition, cetyltrimethylammonium bromide (CTAB) was introduced as a surfactant to control the size and shape of nickel sulfide nanostructures grown in the aqueous hydrazine solution.²⁶ For comparison, the pure Ni₃S₂ was also prepared via a similar way, where the CTAB and aqueous hydrazine were not added. The NiS on Ni foil were also fabricated via the reported method²⁷ and the XRD pattern was shown in Fig. S1†. The X-ray diffraction (XRD) peaks of the obtained samples without the CTAB and aqueous hydrazine can be indexed to the Ni₃S₂ (JCPDS 44-1418). With the CTAB and aqueous hydrazine, the diffraction peaks can be attributed to both Ni₃S₂ and NiS (JCPDS 86-2281) (Fig. 1A). Then, the X-ray photoelectron spectroscopy (XPS) was used to further analyze the chemical valence of the as-prepared samples. Besides the O KLL, Ni LMM, C 1s and O 1s peaks, the S 2s, S 2p, Ni 2s and Ni 3p peaks can be observed in both the Ni₃S₂ and NiS/Ni₃S₂ samples. And no other elemental peaks were observed, indicating that the samples were pure (Fig. 1B). Furthermore, the peak of binding energy of Ni 2p in the NiS/Ni₃S₂ composite is blue-shifted, compared with that of pure Ni₃S₂ (Fig. 1C). Similar phenomena were observed for that of S 2p (Fig. 1D). This demonstrates the oxidation state of the Ni and S changes, arising from the interaction between NiS and Ni₃S₂.

The scanning electron microscope (SEM) was used to study the morphology of the as-prepared composites. Without the CTAB and aqueous hydrazine, the hierarchical dendritic Ni₃S₂ with two long side branches was formed on Ni foil (Fig. 2A). In contrast, in presence of the CTAB and aqueous hydrazine, the NiS/Ni₃S₂ nanorod composite arrays can be obtained (Fig. 2B, C). The length of NiS/Ni₃S₂ nanorod composite array is about 4 μ m (Fig. 2D). In order to further investigate the chemical component of the nanorods, the transmission electron microscope (TEM) was used (Fig. 2E). Further more, the (211) crystal plane of NiS and (101) crystal plane of Ni₃S₂ can be found in the same nanorod (Fig. 2F). The NiS and Ni₃S₂ are well dispersed in the single nanorod. From these data, it can be concluded, to a certain extent, that the NiS/Ni₃S₂ nanorod composite arrays have been prepared.

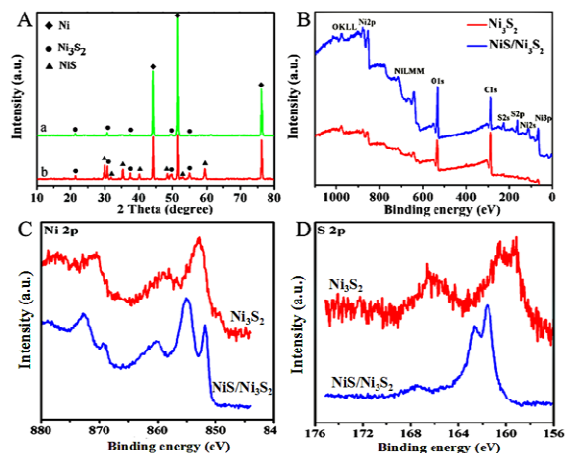


Fig. 1 (A) XRD patterns of the Ni_3S_2 and $\text{NiS}/\text{Ni}_3\text{S}_2$ grown on Ni foil, (B) XPS of the Ni_3S_2 and $\text{NiS}/\text{Ni}_3\text{S}_2$, (C) XPS of Ni 2p of Ni_3S_2 and $\text{NiS}/\text{Ni}_3\text{S}_2$, (D) XPS of S 2p of Ni_3S_2 and $\text{NiS}/\text{Ni}_3\text{S}_2$.

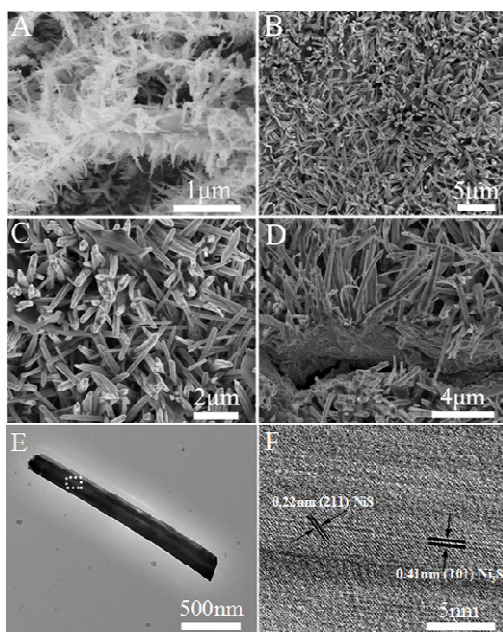


Fig. 2 SEM images of (A) dendritic Ni_3S_2 hierarchical nanostructure, (B, C) $\text{NiS}/\text{Ni}_3\text{S}_2$ nanorod composite arrays, (D) cross-section of $\text{NiS}/\text{Ni}_3\text{S}_2$ nanorod arrays, (E) TEM and (F) HRTEM images of the $\text{NiS}/\text{Ni}_3\text{S}_2$ nanorod composite arrays.

So, the DSSCs with different CEs were fabricated in this work (see details in supporting information). We compared the photocurrent density–voltage (J - V) characteristics of devices based on three CEs (Fig. 3A). The detailed photovoltaic parameters are summarized in Table 1. The DSSCs based on hierarchical Ni_3S_2 show the η of 6.23%, much higher η of 7.20% was achieved by the use of the $\text{NiS}/\text{Ni}_3\text{S}_2$ nanorod composite array in the DSSCs. This efficiency is approaching to that of Pt-based DSSCs (7.56%), and is comparable the reported references (Table S1). One can note that the DSSCs based on nanorod composite array have the highest fill factor (FF), suggesting that the $\text{NiS}/\text{Ni}_3\text{S}_2$ nanorod composite arrays have the lowest diffusion impedance for the redox species.

To further evaluate the catalytic activities and electrons transfer of the $\text{NiS}/\text{Ni}_3\text{S}_2$ nanorod composite arrays, the cyclic voltammetry (CV), electrochemical impedance spectroscopy (EIS) and Tafel

polarization measurements were carried out (Fig. 3B, C, D, respectively). Both the CVs of $\text{NiS}/\text{Ni}_3\text{S}_2$ composite and Pt CEs exhibit two pairs of oxidation and reduction peaks of the I^-/I_3^- redox couple (Fig. 3B). The left pair in the low potential range is assigned as eqn (1) and the right pair in the high potential range as eqn (2). And the cathodic peak of reaction (1) is the most important peak, indicating the reduction of I_3^- at the counter electrode with electrolyte in DSSCs¹⁹.



Apparently, the cathodic and anodic peak current densities of the $\text{NiS}/\text{Ni}_3\text{S}_2$ CEs are higher than that of Pt CEs, indicating that a faster rate for triiodide reduction reaction can be presented, that is, $\text{NiS}/\text{Ni}_3\text{S}_2$ nanorod composite arrays may have higher catalytic activity than Pt. Among all three CEs, the Ni_3S_2 CEs show the poorest catalytic activity. And the $\text{NiS}/\text{Ni}_3\text{S}_2$ nanorod array CE shows stability after consecutive 20 cyclic voltammograms at a scan rate of 25 mV s^{-1} to some extent (Fig. S2†).

The Nyquist plots of EIS for the CEs were carried out with a symmetric cell consisting of two identical CEs (Fig. 3C). And the corresponding parameters are listed in Table 1. According to the equivalent circuit, the high frequency intercept on the real axis represents the series resistance (R_s). The left semicircle in the middle frequency can be attributed to the charge transfer resistance (R_{ct}) and the corresponding capacitance (C_{μ}) at the cathode/electrolyte interface. Nernst diffusion impedance (Z_N) of the redox couple in the electrolyte can be obtained from the low frequency. The R_s values for the DSSCs based on both $\text{NiS}/\text{Ni}_3\text{S}_2$ nanorod composite array and hierarchical Ni_3S_2 are lower than that of Pt, which is caused by the in situ growth of nickel sulfide on Ni foil, then leads to stronger adhesion of nickel sulfide on Ni foil than that of Pt on FTO²³, this allows fast electrons to transfer from nickel sulfides via Ni foil into the external circuit. The R_{ct} value of the DSSCs based on $\text{NiS}/\text{Ni}_3\text{S}_2$ nanorod composite array (1.36Ω) is much lower than that of Ni_3S_2 hierarchical nanostructure (85.03Ω), and is close to that of Pt-based cell (0.79Ω). This result demonstrates that the catalytic activity of $\text{NiS}/\text{Ni}_3\text{S}_2$ composite array is better than that of Ni_3S_2 and is comparable to that of Pt. The Z_N values for $\text{NiS}/\text{Ni}_3\text{S}_2$ and Ni_3S_2 are smaller than that of Pt, demonstrating a fast diffusion velocity of the redox couple (iodide/triiodide) in the systems. These EIS results are consistent with the J - V data.

To further study the catalytic activity of these electrodes, Tafel polarization analysis was performed for the symmetric cells. The limiting current density (J_{lim}) and the exchange current density (J_0) are related to the catalytic activity of the catalysts²⁸. The Tafel curve based on $\text{NiS}/\text{Ni}_3\text{S}_2$ nanorod composite array CE shows a larger slope than that for Pt and hierarchical Ni_3S_2 CE, indicating a higher J_0 , a higher J_0 means that $\text{NiS}/\text{Ni}_3\text{S}_2$ CE has better catalytic activity for I_3^- reduction. In eqn (3), R_{ct} is the charge-transfer resistance obtained from EIS, R is the gas constant and F is Faraday's constant. In addition, the J_{lim} for $\text{NiS}/\text{Ni}_3\text{S}_2$ CE is higher than that for Pt and Ni_3S_2 CE (eqn (4)). In the equation, D is the diffusion coefficient of I_3^- , l is the spacer thickness, C is the I_3^- concentration, N_A is Avogadro's constant, and e and n have their usual meanings.

$$J_0 = RT / nFR_{ct} \quad (3)$$

$$J_{lim} = 2neDCN_A / l \quad (4)$$

As a comparison, the photoelectrochemical performance of DSSCs based on NiS CEs was also investigated (Fig. S3†). It can be seen that the η of DSSCs based on NiS CEs is lower than those based on hierarchical Ni_3S_2 and $\text{NiS}/\text{Ni}_3\text{S}_2$ nanorod CEs, It is because NiS CEs have lower catalytic activity and slower electron transfer. The CV, EIS and Tafel test can verify it.

In order to further identify that the NiS/Ni₃S₂ is more beneficial for the electron transfer than Ni₃S₂, the Scanning Kelvin Probe (SKP) measurement was taken (Fig. 3E, F). It can be seen that the SKP potential of NiS/Ni₃S₂ is higher than that of Ni₃S₂. After calculation, the work function of NiS/Ni₃S₂ is 5.18 eV, which is comparable to that of Pt (5.65 eV) and is higher than that of Ni₃S₂ (5.11 eV). The work function changes due to the formation of composite array. This will result in the increased built-in field, which favors the fast photoelectron transfer across the hybrids into the interface of NiS/Ni₃S₂ composite array and I₃⁻/I⁻ redox shuttle. So, the NiS/Ni₃S₂ composite is more favorable for the electron transfer than Ni₃S₂ and shows comparable catalytic activity to Pt (Fig. S4†). Therefore, the NiS/Ni₃S₂ nanorod composite array CE displays high catalytic activity, and DSSCs based on it get high η that is comparable to that of Pt CE. Considering the higher light reflectance of Pt electrode than that of NiS/Ni₃S₂, the increased light reflectance is of advantage to reduce the losses of the light, which could remarkably improve the efficiency. Similar phenomenon has been demonstrated in some reported works^{8,29}. In considering its high η and simple synthesized method, the NiS/Ni₃S₂ CE may be an effective alternative to Pt CE for DSSCs.

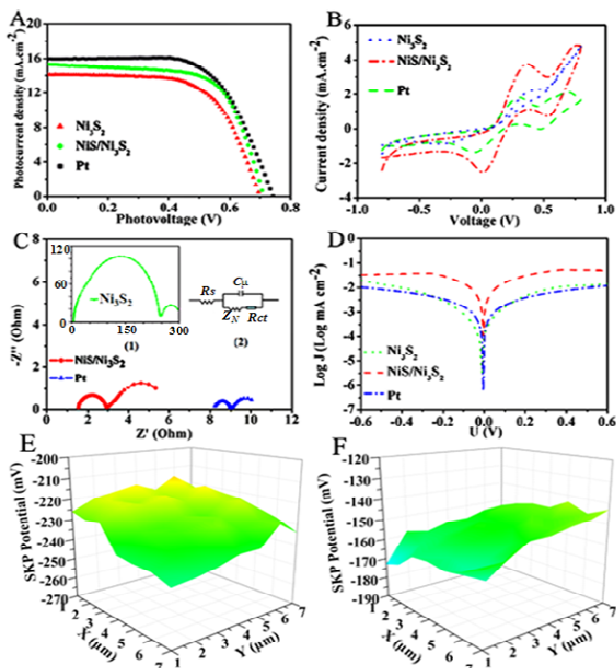


Fig. 3 (A) J - V characteristics of DSSCs with different CEs, (B) Cyclic voltammograms for the series of CEs at a scan rate of 25 mV s⁻¹, (C) Nyquist plots of different symmetric cells (inset: a fitted equivalent circuit), (D) Tafel-polarization curves of the symmetric cells, SKP potential images of (E) Ni₃S₂ CE and (F) NiS/Ni₃S₂ CE.

Table 1. Photovoltaic parameters of DSSCs with different CEs

DSSCs	V_{oc}/V	$J_{sc}/\text{mA cm}^{-2}$	FF	$\eta/\%$	R_s/Ω	R_{ct}/Ω	$C_{\mu}/\mu\text{F}$	Z_N/Ω
CNi ₃ S ₂	0.70	14.13	0.63	6.23	5.26	85.03	12.30	0.65
CNiS/Ni ₃ S ₂	0.71	15.33	0.66	7.20	1.54	1.36	12.50	0.36
C _{Pt}	0.74	15.95	0.64	7.56	8.20	0.79	22.60	1.23

Conclusions

In summary, the NiS/Ni₃S₂ nanorod composite array CE has been fabricated via a facile hydrothermal method. Its electrocatalytic activity was revealed to be the highest among the three CEs. The

composite CE displays faster electron transport than Pt and Ni₃S₂ CEs. Consequently, these allow for the high photoelectrical conversion efficiency, approaching to that of Pt-based cell. Therefore, the in situ fabricated NiS/Ni₃S₂ nanorod composite array CE may be a good candidate for high efficiency and low-cost DSSCs.

We gratefully acknowledge the support of the NSFC (21376065, 51272070), Innovative Research Team of MOE (IRT-1237), New Century Excellent Talents (NCET-11-0958, NCET-11-0959).

Notes and references

Key Laboratory of Functional Inorganic Material Chemistry, Ministry of Education, Heilongjiang University, Harbin 150080, People's Republic of China. Tel.: +86 451 8660 9141; fax: +86 451 8667 3647; E-mail: kaipan@hlju.edu.cn, fuhg@vip.sina.com

† Electronic supplementary information (ESI) available: See DOI:

- B. O'Regan and M. Grätzel, *Nature*, 1991, **353**, 737–740.
- M. Grätzel, *Nature*, 2001, **414**, 338–344.
- J. H. Li and J. Z. Zhang, *Coord. Chem. Rev.*, 2009, **253**, 3015–3041.
- M. X. Wu, X. Lin, Y. D. Wang, L. Wang, D. D. Qi, X. J. Peng, A. Hagfeldt, M. Grätzel and T. L. Ma, *J. Am. Chem. Soc.*, 2012, **134**, 3419–3428.
- G. Smestad, C. Bignozzi and R. Argazzi, *Sol. Energy Mater. Sol. Cells*, 1994, **32**, 259–272.
- H. Wang, K. Sun, F. Tao, D. J. Stacchiola and Y. H. Hu, *Angew. Chem. Int. Ed.*, 2013, **125**, 9380–9384.
- H. C. Sun, Y. H. Luo, Y. D. Zhang, D. M. Li, Z. X. Yu, K. X. Li and Q. B. Meng, *J. Phys. Chem. C*, 2010, **114**, 11673–11679.
- X. H. Miao, K. Pan, Q. J. Pan, W. Zhou, L. Wang, Y. P. Liao, G. H. Tian and G. F. Wang, *Electrochim. Acta.*, 2013, **96**, 155–163.
- H. W. Zhou, Y. T. Shi, L. Wang, H. Zhang, C. Y. Zhao, A. Hagfeldt and T. L. Ma, *Chem. Commun.*, 2013, **49**, 7626–7628.
- R. Bajpai, S. Roy, N. Koratkar and D. S. Misra, *Carbon*, 2013, **56**, 56–63.
- G. R. Li, F. Wang, Q. W. Jiang, X. P. Gao and P. W. Shen, *Angew. Chem., Int. Ed.*, 2010, **49**, 3653–3656.
- Y. P. Liao, K. Pan, L. Wang, Q. J. Pan, W. Zhou, X. H. Miao, B. J. Jiang and H. G. Fu, *ACS Appl. Mater. Interfaces*, 2013, **5**, 3663–3670.
- C. W. Kung, H. W. Chen, C. Y. Lin, K. C. Huang, R. Vittal and K. C. Ho, *ACS Nano*, 2012, **6**, 7016–7025.
- Q. Wang, R. Gao and J. H. Li, *Appl. Phys. Lett.*, 2007, **90**, 143107.
- X. H. Miao, K. Pan, G. F. Wang, Y. P. Liao, L. Wang, W. Zhou, B. Jiang, Q. Pan, Y. Xie and G. Tian, *Chem. Eur. J.*, 2014, **20**, 474–482.
- J. Yang, C. X. Bao, K. Zhu, T. Yu, F. M. Li, J. G. Liu, Z. S. Li and Z. G. Zou, *Chem. Commun.*, 2014, **50**, 4824–4826.
- Y. B. Li, H. F. Wang, H. M. Zhang, P. R. Liu, Y. Wang, W. Q. Fang, H. G. Yang, Y. Li and H. J. Zhao, *Chem. Commun.*, 2014, **50**, 5569–5571.
- S. Krishnakumar, N. Shanthy and D. Sarma, *Phys. Rev. B: Condens. Matter Mater. Phys.*, 2002, **66**, 115101–115106.
- H. C. Sun, D. Qin, S. Q. Huang, X. Z. Guo, D. M. Li, Y. H. Luo and Q. B. Meng, *Energy Environ. Sci.*, 2011, **4**, 2630–2637.
- H. K. Mulmudi, S. K. Batabyal, M. Rao, N. Mathews, Y. M. Lam and S. G. Mhaisalkar, *Phys. Chem. Chem. Phys.*, 2011, **13**, 19307–19309.
- W. J. Ke, G. J. Fang, H. Tao, P. L. Qin, J. Wang, H. W. Lei, Q. Liu and X. Z. Zhao, *ACS Appl. Mater. Interfaces*, 2014, **6**, 5525–5530.
- W. Zhao, X. L. Zhu, H. Bi, H. L. Cui, S. R. Sun and F. Q. Huang, *J. Power Sources*, 2013, **242**, 28–32.
- W. Zhao, T. Q. Lin, S. R. Sun, H. Bi, P. Chen, D. Y. Wan and F. Q. Huang, *J. Mater. Chem. A*, 2013, **1**, 194–198.
- Y. Hou, D. Wang, X. Yang, W. Fang, B. Zhang, H. Wang, G. Lu, P. Hu, H. Zhao and H. Yang, *Nat. Commun.*, 2013, **4**, 1583–1590.
- Y. Tachibana, L. Vayssieres, J. R. Durrant, *Nat. Photonics* 2012, **6**, 511–518.
- L. Z. Zhang, J. C. Yu, M. S. Mo, L. Wu, Q. Li and K. W. Kwong, *J. Am. Chem. Soc.*, 2004, **126**, 8116–8117.
- W. S. Chi, J. W. Han, S. Yang, D. Y. Roh, H. Lee and J. H. Kim, *Chem. Commun* 2012, **48**, 9501–9503.
- M. X. Wu, X. Lin, A. Hagfeldt and T. L. Ma, *Angew. Chem. Int. Ed.* 2011, **50**, 3520–3524.
- Z. Huang, X. Z. Liu, K. X. Li, D. M. Li, Y. H. Luo, H. Li, W. B. Song, L. Q. Chen and Q. B. Meng, *Electrochem. Commun.*, 2007, **9**, 596–598.